

## Article

# Cold Sintering Process of Zinc Oxide Ceramics: Powder Preparation and Sintering Conditions Effects on Final Microstructure

Andrey V. Smirnov <sup>1</sup>, Maxim V. Korniyushin <sup>1,2</sup>, Anastasia A. Kholodkova <sup>1,3,\*</sup> , Sergey A. Melnikov <sup>2</sup>, Artem D. Stepanov <sup>2</sup>, Elena V. Fesik <sup>4</sup>  and Yurii D. Ivakin <sup>1,3</sup>

<sup>1</sup> Mobile Solutions Engineering Center, MIREA-Russian Technological University, 119454 Moscow, Russia

<sup>2</sup> Materials Science Department, Moscow Polytechnic University, 107023 Moscow, Russia

<sup>3</sup> Chemistry Department, M. V. Lomonosov Moscow State University, 119991 Moscow, Russia

<sup>4</sup> M.V. Lomonosov Institute of Fine Chemical Technologies, MIREA-Russian Technological University, 119454 Moscow, Russia

\* Correspondence: anastasia.kholodkova@gmail.com

**Abstract:** Although the activating effect of an acetate medium in the cold sintering process of zinc oxide ceramics is well known, some problems need to be solved on the effect of process conditions and the initial powder's preparation methods on the ceramic's density and microstructure. This article describes an effect of the zinc acetate introduction method, its concentration in zinc oxide powder as well as that of the die sealing configuration on the density and microstructure of zinc oxide ceramics obtained by the cold sintering process at 244 °C. The activating additive of zinc acetate was applied in two ways: (1) impregnation in aqueous solution and (2) impregnation with subsequent treatment in water vapor. Zinc oxide powders and ceramics were analyzed using SEM, TGA/DSC/MS and XRD to reveal the effect of powder pre-treatment and sintering conditions on the material microstructure. Cold sintered ZnO ceramics samples with a relative density up to 0.99 and with average grain sizes from 0.28 to 1.71 μm were obtained. The die sealing by two Teflon sealing rings appeared to be the most effective.

**Keywords:** oxide ceramics; zinc oxide; cold sintering process; thermo-vaporous treatment; microstructure



**Citation:** Smirnov, A.V.; Korniyushin, M.V.; Kholodkova, A.A.; Melnikov, S.A.; Stepanov, A.D.; Fesik, E.V.; Ivakin, Y.D. Cold Sintering Process of Zinc Oxide Ceramics: Powder Preparation and Sintering Conditions Effects on Final Microstructure.

*Inorganics* **2022**, *10*, 197. <https://doi.org/10.3390/inorganics10110197>

Academic Editor: Sergey Kuznetsov

Received: 25 September 2022

Accepted: 3 November 2022

Published: 5 November 2022

**Publisher's Note:** MDPI stays neutral with regard to jurisdictional claims in published maps and institutional affiliations.



**Copyright:** © 2022 by the authors. Licensee MDPI, Basel, Switzerland. This article is an open access article distributed under the terms and conditions of the Creative Commons Attribution (CC BY) license (<https://creativecommons.org/licenses/by/4.0/>).

## 1. Introduction

The cold sintering process (CSP) is currently one of the hottest topics in ceramics applied and fundamental science [1]. The CSP was developed at Pennsylvania State University, USA starting from 2016 in order to reduce the energy consumed and the carbon footprint generated by ceramics manufacturing [2]. Usually, the CSP is carried out as follows: a mixture of powders and a liquid phase (usually acid–water solutions) is uniaxially pressed (50–500 MPa) within a die at a temperature below 400 °C [3]. Also, spark plasma sintering (SPS) systems can be adapted to reproduce CSP [4,5].

One of the key issues for CSP is controlled liquid evaporation. The liquid is a metastable transient phase which tends to evaporate from the die over time during the CSP. If the porosity is completely filled by liquid, the driving force for densification is nullified; therefore, densification cannot take place unless water is removed from the system. Conversely, if the evaporation is too fast, water is completely removed from the die before sintering is concluded, thus impeding further densification [6]. These days, the lack of information about the effect of the water evaporation rate and the required amount of liquid for CSP is an investigators' problem that needs to be solved. The authors of recent review articles [1,6] mentioned that the water evaporation control is a key challenge for CSP future developments and possible industrial scale-up. In particular, a systematic study of the effect of the pressing system (die/punch) clearance on CSP is still missing with the

exception of the preliminary results of several experimental works [7,8]. The mold sealing can have a significant impact on the densification and grain growth during CSP. With complete sealing, on one hand, hydrothermal conditions occur during the entire time of the process, with partial sealing; on the other hand, the CSP conditions will be more complex and will change along with the gradual evaporation of water.

Another important issue in CSP, which remains unclear at the moment, is the method of introducing additives that activate sintering. The prevailing description of the CSP mechanism is based on the mass transfer due to dissolution–precipitation of oxide particles in the environment called the transport medium. Usually, water or acidic aqueous solutions play the role of this medium. However, there are studies of CSP conducted without the addition of liquid water. For example, ZnO ceramics were processed in the presence of zinc acetate dihydrate without any other sources of water in the medium but for residual moisture and the amount of water adsorbed during preliminary exposure of the initial powder to a humid environment [9]. These results are questioning the predominance of the dissolution–precipitation mechanism in CSP. The decisive role of water in the oxide ceramics CSP is undeniable, but the mechanism of its action is still not fully discovered. Certain substances called sintering activators are known to facilitate the CSP when introduced into the reaction medium [10,11]. In most cases, acetate anions are used as an activator for ZnO sintering. Earlier [4,12], the changes in the dispersion of ZnO powder under the conditions of both autoclave treatment and CSP were reported. These changes were caused by mass transfer in a closed volume and occurred with the participation of water molecules. The mechanisms of mass redistribution between ZnO crystals should have the same stages under the considered conditions.

It was assumed that the application of zinc acetate  $\text{Zn}(\text{CH}_3\text{COO})_2$  (AcZn) by the impregnation method would not change the state of ZnO crystals, but form on the surface zinc cations, protons and acetate anions, as well as hydroxyl groups adsorbed from an aqueous solution due to dissociative adsorption of water molecules.

When processing ZnO in an autoclave in a water vapor medium (thermo-vapor treatment (TVT), the presence of AcZn leads to changes in both the shape of crystals and their size distribution, i.e., it is accompanied by a rearrangement of the initial crystals, as well as mass transfer between crystals and formation of the fine crystals [13]. These changes occur by a solid-phase mechanism due to the appearance of the mobility of the crystal structure due to interaction with the aqueous medium [11] with the initial hydroxylation of the crystal volume and the improvement of the crystal structure [4]. Two methods of preparing ZnO powder for CSP transfer the initial powder to a different state. It was assumed that the improvement of the crystal structure by TVT and the appearance of solid-phase mobility by the impregnation method may have different effects on the CSP. It was also found that the rapid (dwell time 5 min, heating time about 2 min) CSP/SPS of ZnO is affected by the method of activator introduction into the initial powder [4]. In conventional long-term CSP (dwell time 60 min, heating time 40 min) without SPS rapid heating, no difference between impregnation or injecting methods of acetate additive introduction was observed [14].

The purpose of this work was to compare the effectiveness of the ZnO conventional long-term CSP activation with two methods of AcZn. Stages of investigation: (1) simple application of the activator by impregnation followed by powder drying and (2) by the activator impregnation followed by powders autoclave thermo-vapor treatment (TVT). In addition, the influence of the die sealing configuration and material (PTFE or copper) was investigated.

## 2. Results

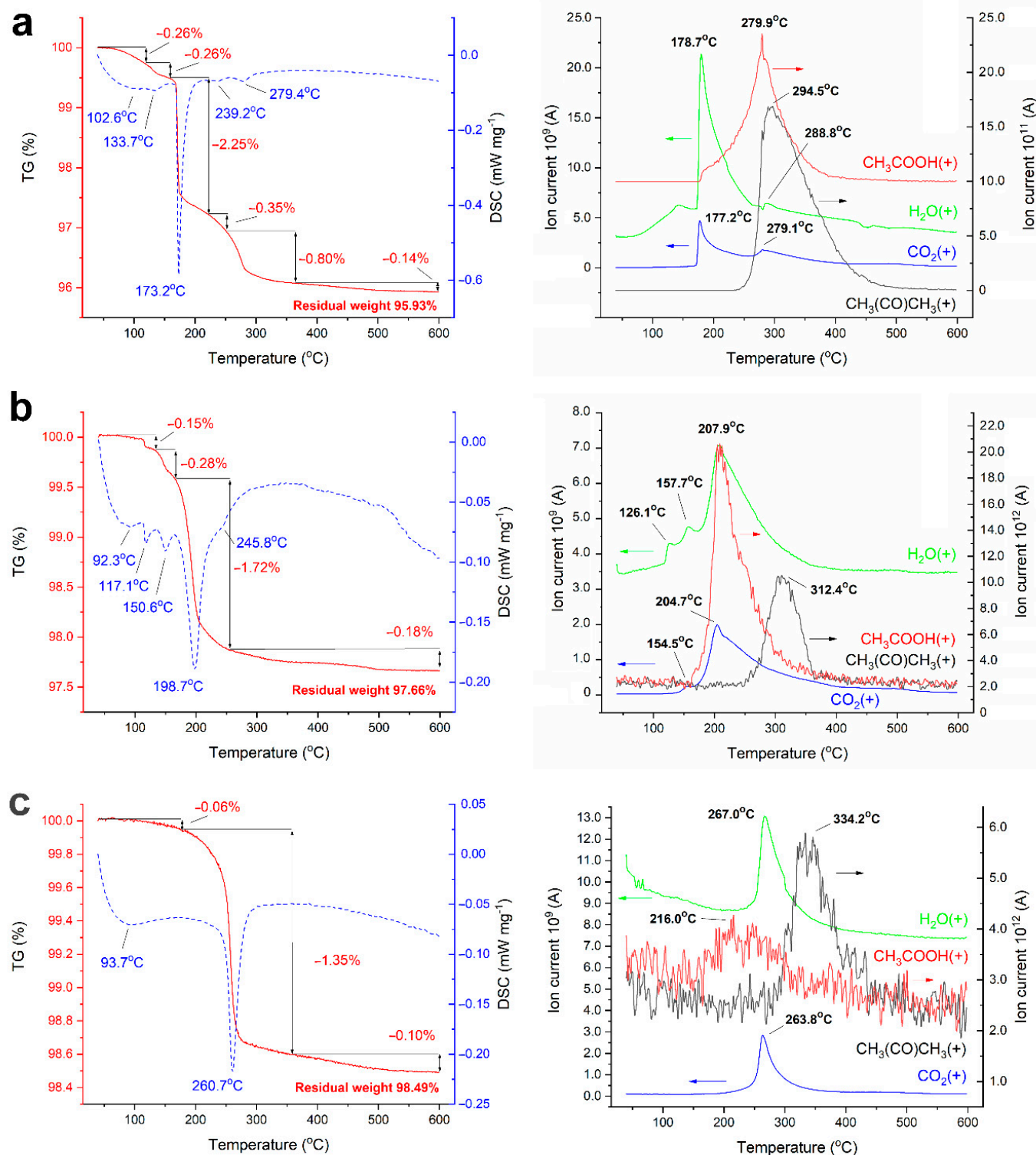
### 2.1. Initial ZnO Powder Recrystallization after ZnAc Introduction

The application of AcZn to ZnO by the impregnation method leads, as previously established [4], to the formation of  $Zn_5(OH)_8(CH_3COO)_2 \cdot 2H_2O$  (layered basic zinc acetate, (LBZA)) [15]. This phase is unstable and decomposes after TVT and CSP. Figure 1 shows the results of TGA/DSC/MS in the argon flow of powders with 5 wt.% AcZn impregnated ( $ZnO@AcZn(5\%)$ ), as well as after TVT ( $ZnO@AcZnTVT(5\%)$ ) and CSP ( $CSP ZnO@AcZnTVT(5\%)$ ).

The mass loss of the impregnated ZnO powder sample  $ZnO@AcZn(5\%)$  has four stages (Figure 1a). At the first stage, adsorbed water is released at temperatures up to 150 °C with a wide endothermic peak and a mass loss of 0.52%. Further, the main mass loss 2.25% occurs during the dehydration of AcZn, which is accompanied by an endoeffect at 173 °C and a small release of  $CO_2$ . At the next temperature stage at 240–280 °C decomposition of the acetate group is observed with the formation of acetic acid first, then acetone and a total mass loss of 1.15%. A small mass loss of 0.14% at the last stage at temperature above 350 °C is mainly due to the release of water.

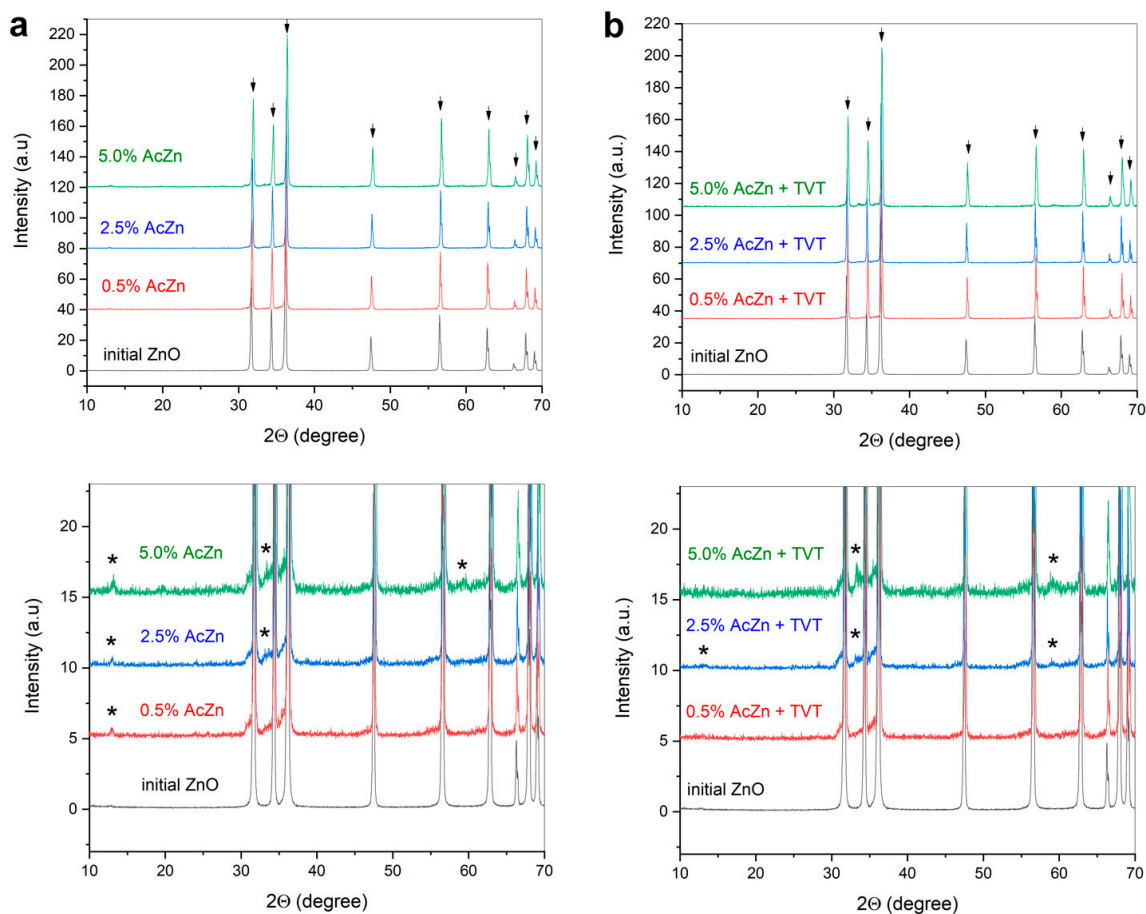
After TVT of ZnO powder at 220 °C, the thermal processes change (Figure 1b). The mass loss of the sample  $ZnO@AcZnTVT(5\%)$  has three temperature stages. The release of water at the first stage is accompanied by narrow endothermic effects at 117 °C and 151 °C, which correspond to two maxima of water flow with a mass loss of 0.15% and 0.28%. The main mass loss of 1.72% with an endoeffect at 199 °C occurs with the simultaneous release of water, acetic acid,  $CO_2$  and the same profile of gas flows; on the decline of this, at a temperature of about 300 °C, acetone is released. The nature of the release of  $H_2O$ ,  $CH_3COOH$  and  $CO_2$  indicates the decomposition of some associate of hydroxyls and an acetate group, followed by the formation of acetone. At the third temperature stage above 350 °C, an insignificant amount of water is released. It should be noted that the wide endothermic effect at 92 °C corresponds to the release of adsorbed water, and the narrow effects at 117 °C and 151 °C refer to the beginning of the decomposition of the associate, because at 150 °C the release of  $CH_3COOH$  and  $CO_2$  begins. Thus, the entire weight loss of 2.34% can be attributed to the water–acetate associate.

The weight loss of  $ZnO@AcZnTVT-CS$  ceramics is reduced by a factor of 1.5 compared to  $ZnO@AcZnTVT$  powder before sintering. At the beginning of the heating process, the release of weakly adsorbed water accompanied by a wide endothermic effect at 94 °C is retained, while other two effects corresponding to the release of more strongly bounded water are not observed. The temperature of the main weight loss rises from 199 °C to 261 °C. The destruction of the associate noted above occurs in the temperature range of 150–400 °C. However, when comparing the mass spectra of gas flows, it can be seen that the decrease in the total mass loss is mainly due to the lower release of acetic acid and acetone. This can also be seen in a decrease in the contribution to the endothermic effect, which was previously observed at 246 °C. In this case, the temperature of their release maximum increases by about 20 °C, while for  $CO_2$  and water flows the shift is about 60 °C. Consequently, after CSP, water is more strongly bonded in the associate in the form of hydroxyls. Associate decomposition leads to the formation of  $CO_2$  and elimination of these hydroxyl groups in the form of water. After the release of structural hydroxyls from the residues of the acetate group, acetone is formed and, possibly, acetic acid in a smaller amount.



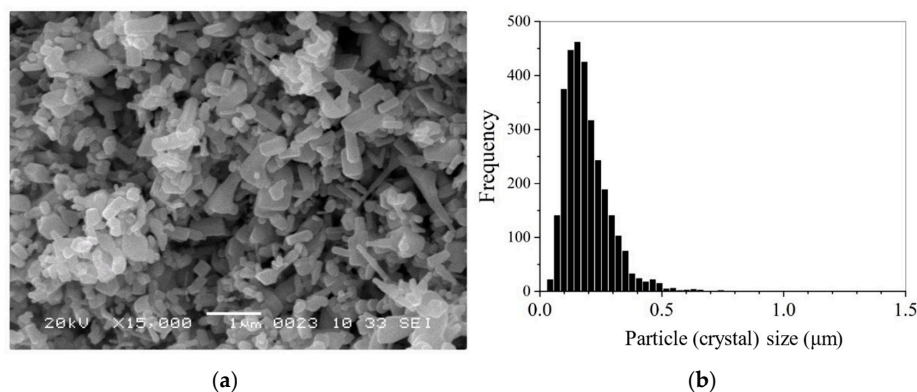
**Figure 1.** TGA/DSC/MS curves of ZnO@AcZn(5%) (a), ZnO@AcZnTVT(5%) (b), CSP ZnO@AcZnTVT(5%) (c).

Phase analysis of the starting powder (Figure 2) revealed correspondence of its structure to zincite (Crystallography Open Database [16] (COD) #9008877). Impregnation by ZnAc as well as TVT provided no essential differences between phase contents of the obtained samples and the initial ZnO. Probably, traces of the LBZA decomposition were found, which could not be identified due to the low intensity of reflexes.

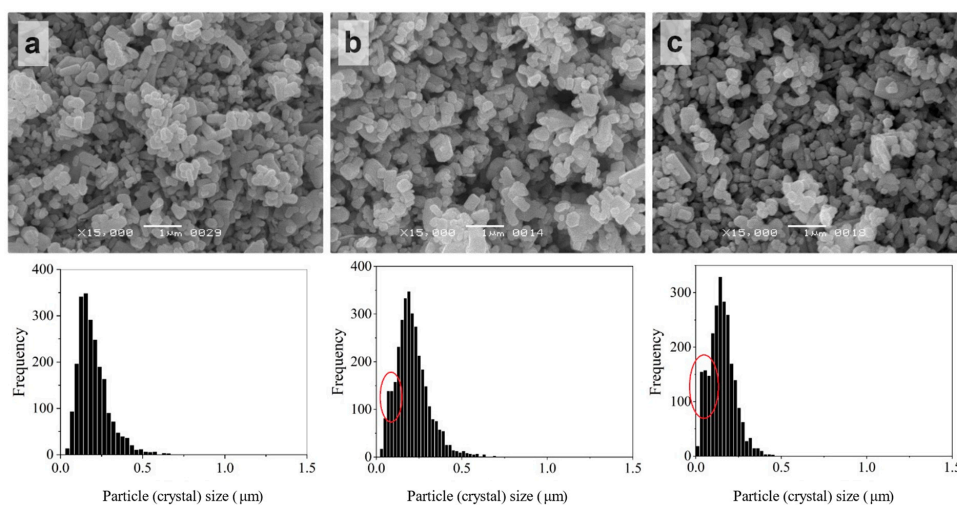


**Figure 2.** XRD patterns of initial ZnO powder, ZnO powders impregnated by 0.5–5.0 wt.% ZnAc (a), ZnO powders after impregnation by 0.5–5.0 wt.% ZnAc followed by TVT (b). Arrows indicate ZnO (COD #9008877), asterisk indicated traces of the LBZA (probably).

The initial ZnO crystals possessed different habitus and mainly the size range was at 0–0.5  $\mu\text{m}$  with a median of  $0.174 \pm 0.002 \mu\text{m}$  (Figure 3). After impregnation by ZnAc (ZnO@ZnAc), thin elongated crystals disappeared, but the size range of the powder crystals was preserved. At the same time, an increase of ZnAc amount in the powder from 0.5 to 2.5 wt.% was accompanied by an increase in the proportion of small crystals (Figure 4). First it appeared as a shoulder on the left wing of the histogram (circled at Figure 4b), and then as an obvious fine component of size distribution (circled at Figure 4c).

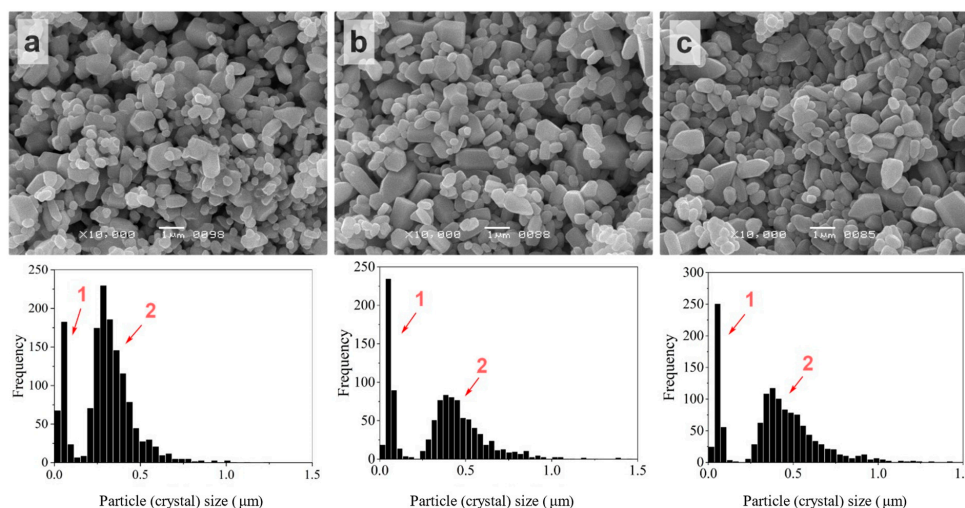


**Figure 3.** SEM image (a) and crystal size distribution (b) of the initial ZnO powder. Mean size  $d_{mn} = 0.193 \pm 0.002 \mu\text{m}$ , median size  $d_{md} = 0.174 \pm 0.002 \mu\text{m}$ .



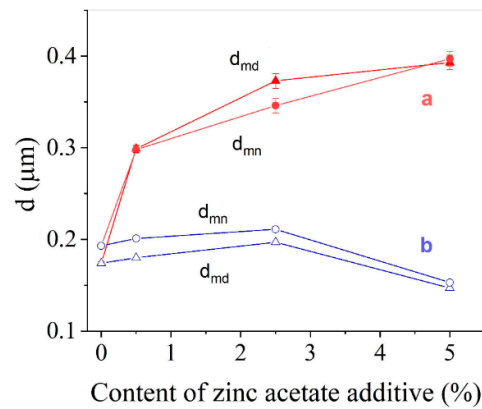
**Figure 4.** SEM images and crystal size distributions of ZnO powder after ZnAc introduction by impregnation: ZnO@AcZn(0.5%) (a), ZnO@AcZn(2.5%) (b), ZnO@AcZn(5%) (c).

The TVT of impregnated powders (ZnO@ZnAcTVT) led to a pronounced change in crystal size distribution for each concentration of the activator (Figure 5). The initial histogram split into fine and coarse components noted as 1 and 2 in Figure 5, correspondingly. The coarse component shifted to higher sizes compared to the starting ZnO. Moreover, the crystals of ZnO@ZnAcTVT acquired a rounded shape. The size range of the fine component has not changed. For a sample with 5% AcZn, the fine component was 0.034 wt.% of the crystal's coarse component.



**Figure 5.** SEM images and crystal size distributions of ZnO powder after ZnAc introduction by impregnation combined with TVT: ZnO@AcZnTVT(0.5%) (a), ZnO@AcZnTVT(2.5%) (b), ZnO@AcZnTVT(5%) (c). 1 and 2 indicated fine and coarse components of size distributions, correspondingly.

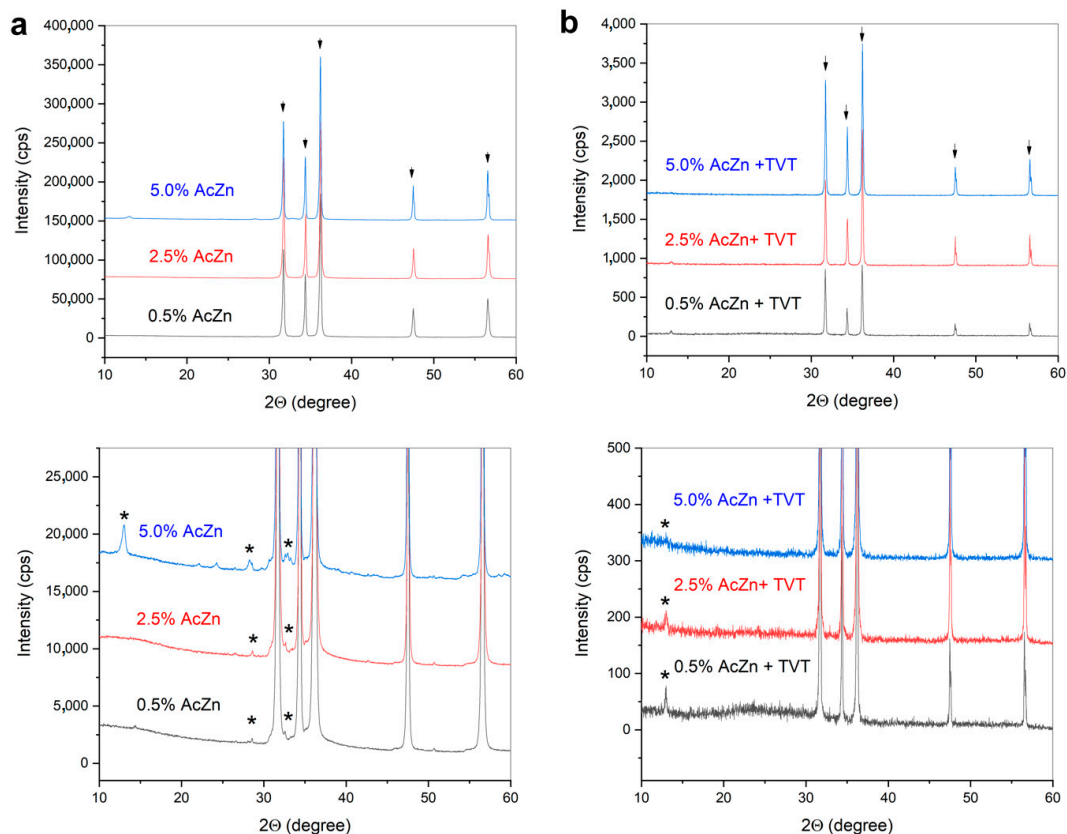
Figure 6 showed the change in the average ZnO crystal size with the increase of ZnAc content for two methods of powder activation. Impregnation combined with TVT leads to gradual growth of mean and median crystal sizes with the increase of ZnAc. Due to the addition of 5.0 wt.% of ZnAc, the crystal size of powder increased twice compared to the initial ZnO. This crystal growth originates from the formation of the coarse component of the size distribution (Figure 5). In contrast, when the powder was only impregnated, the average crystal size, as well as median, decreased because of the formation of a fine component in its size distribution.



**Figure 6.** Mean crystal size ( $d_{mn}$ ) and median ( $d_{md}$ ) of the size distribution of activated ZnO powder vs. ZnAc content for two types of activation: impregnation by ZnAc followed by TVT (a); impregnation by ZnAc (b).

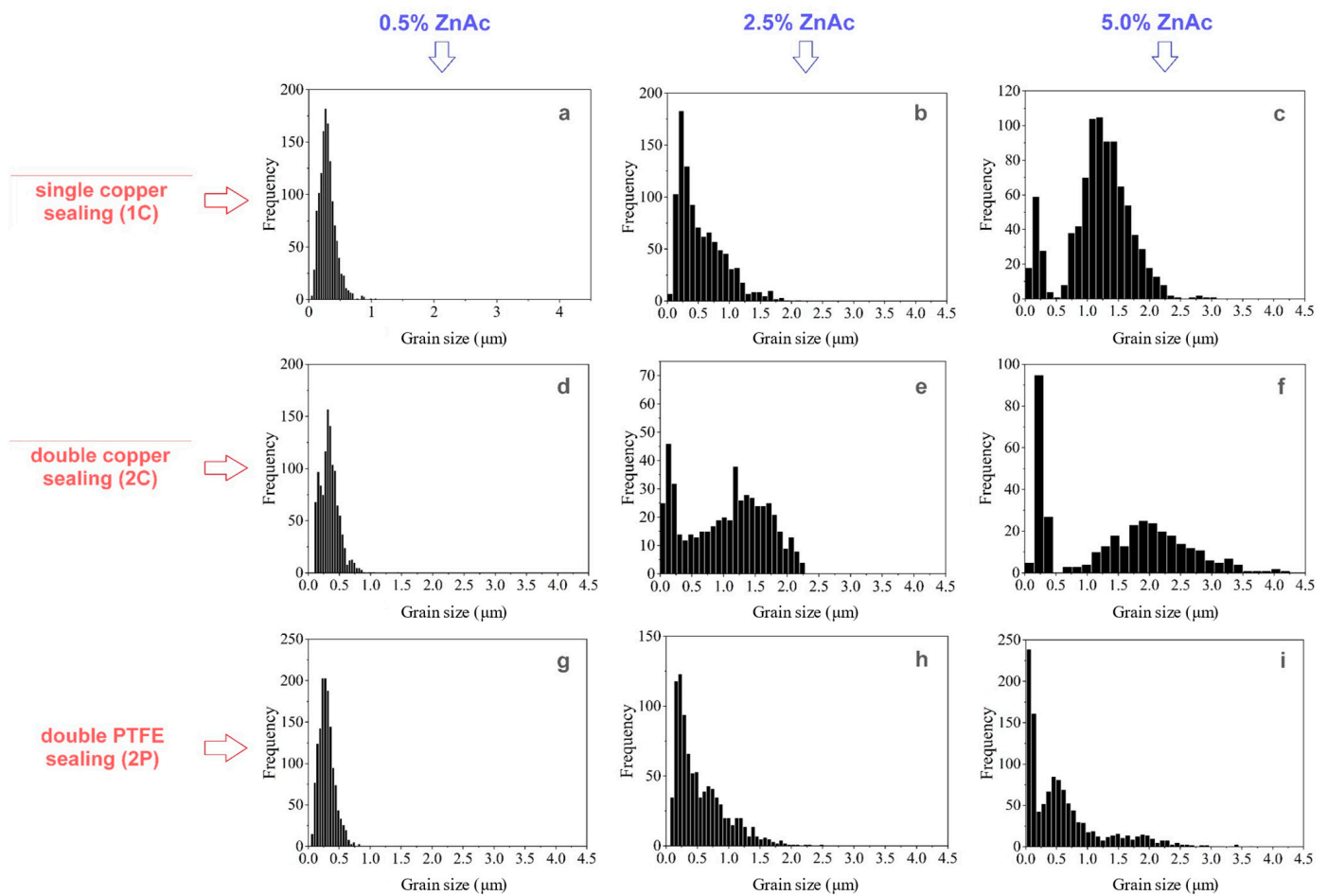
## 2.2. CSP Ceramics Microstructure and Density

XRD analysis of ZnO ceramics prepared by CSP from impregnated powders, as well as those impregnated in combination with TVT (Figure 7), showed their phase content mostly corresponded to zincite (COD #9008877). Besides the intensive peaks of ZnO, weak ones of the unidentified decomposition product of the LBZA phase are marked with an asterisk.

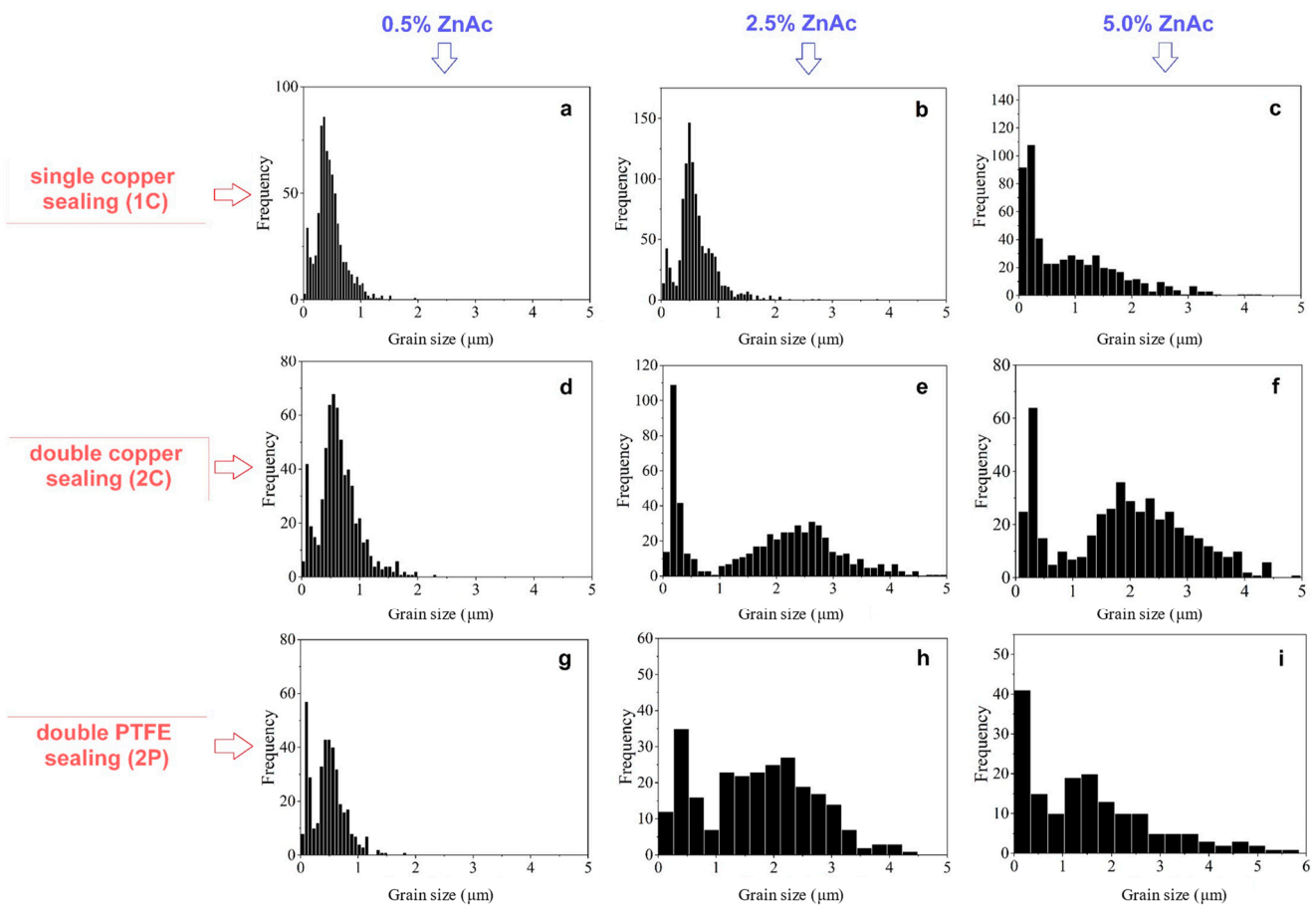


**Figure 7.** XRD patterns of ZnO ceramics prepared by CSP with double PTFE sealing from ZnO powders impregnated by 0.5–5.0 wt.% ZnAc, (a), ZnO powders after impregnation by 0.5–5.0 wt.% ZnAc followed by thermo-vapor treatment (TVT) (b). The ceramics were prepared with double PTFE sealing of the die (2P). Arrows indicate ZnO (COD #9008877), asterisk indicated traces of the LBZA (probably).

The effect of the die sealing mode and ZnAc concentration on grain size distribution in the ceramics prepared by CSP is shown in Figures 8 and 9 for the impregnated and TVT powders, correspondingly. Comparison of the grain size distribution revealed no noticeable grain growth during CSP with addition of 0.5 wt.% ZnAc regardless the method of ZnO activation as well as the die sealing mode: no sealing (1C), double copper sealing (2C), double PTFE sealing (2P). Grain growth and pronounced changes in the grain size distributions became noticeable when ZnAc content increased up to 2.5 wt.% and enhanced in case of 5.0 wt.% of ZnAc. A common feature of the considered series of ceramic samples with increasing ZnAc content was an evolution of grain size distribution from narrow mono-component profile to two distinguished components through an asymmetric histogram. When the ZnO@ZnAc powder was treated in TVT conditions, two components of grain size distributions were observed for all concentrations of the activator (Figure 9). This fact, as well as the appearance of two size components at TVT and CSP of ZnO@AcZn powders, indicates the same influence of the aqueous medium on the crystal's and grain's size evolution in the processes of TVT and CSP. A feature of this evolution is an increase in the size range of the fine component with a noticeable increase in the size of the coarse component (from ~0–0.2  $\mu\text{m}$  to ~0–0.5 and 0–1  $\mu\text{m}$ ). For CSP samples with the addition of 5% AcZn and 2P sealing, the mass fraction of the fine component was 0.029 wt.% of the coarse component when powder-activated by impregnation and 0.045 wt.% when activated by TVT.

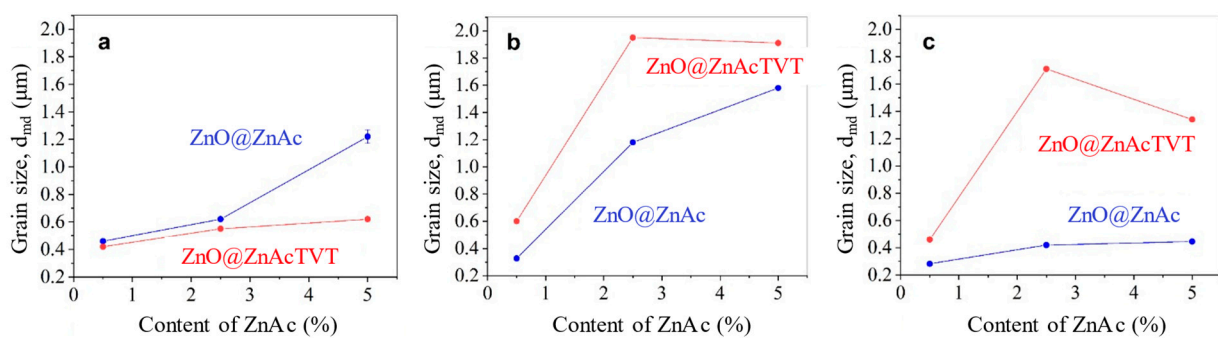


**Figure 8.** Grain size distributions of ceramics prepared from ZnO powder impregnated by 0.5 wt.% of ZnAc (a,d,g), 2.5 wt.% of ZnAc (b,e,h) and 5.0 wt.% of ZnAc (c,f,i) after CSP with the use of different types of sealing.



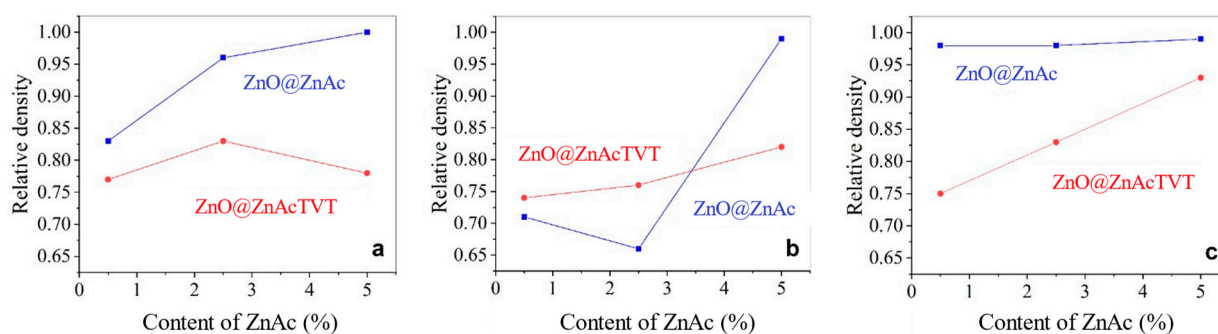
**Figure 9.** Grain size distributions of ceramics prepared from ZnO powder activated by impregnation and TVT (a,d,g—0.5 wt.% of ZnAc; b,e,h—2.5 wt.% of ZnAc; c,f,i—5.0 wt.% of ZnAc) after CSP with the use of different types of sealing.

The changes of the median grain size distribution in the CSP samples obtained with different methods of the implementing ZnAc and the die sealing are shown in Figure 10. Grain growth observed with no sealing (1C) (Figure 10a) significantly increased with maximum sealing type 2C (Figure 10b). The median of grain size distribution raised in both cases of powder activation, by impregnation as well as TVT. The use of 2P sealing resulted in moderate grain growth (Figure 10c).



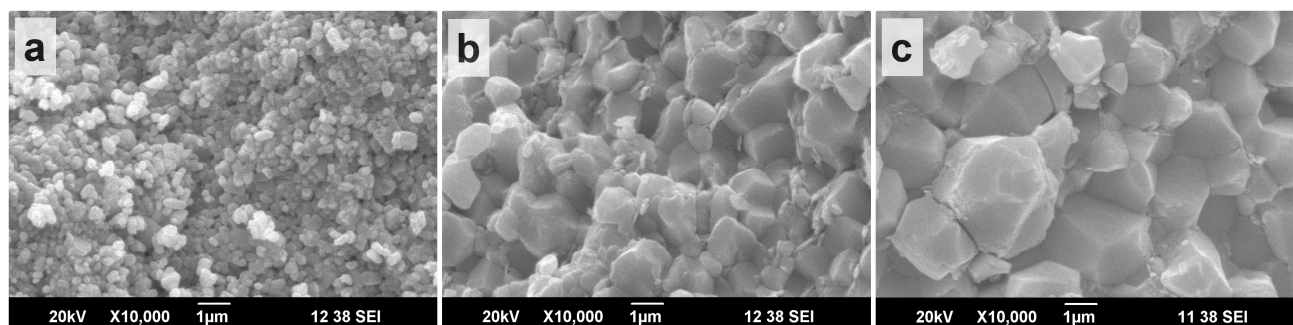
**Figure 10.** Median of grain size distribution of ZnO ceramics vs. ZnAc concentration for different types of sealing during CSP: single copper sealing 1C (a); double copper sealing, 2C (b); double PTFE sealing, 2P (c). Initial ZnO powder activation: ZnO@ZnAc-impregnation; ZnO@ZnAcTVT-impregnation followed by TVT.

Figure 11 showed the change in the relative density of CSP samples. In general, the growth of crystalline grains with an increase of the ZnAc content resulted in densification of ceramic samples. The highest relative density (over 0.95) was achieved due to the introduction of 5.0 wt.% ZnAc by impregnation for all three types of sealing (1C, 2C, 2P). The exception appeared in the series of samples manufactured from ZnO@ZnAcTVT powder with single copper sealing (Figure 11a). This could be explained by poor reproducibility of vapor pressure in the case of 1C sealing because of uncontrollable water leakage from the die. At the same time, PTFE sealing allows the relative density over 0.95 to be achieved at any of the ZnAc concentrations considered for the series of ZnO@ZnAc. The influence of the sealing type on the relative density of the ZnO was clearly showed in the samples produced from ZnO@ZnAcTVT powder. Especially if die was sealed with two PTFE rings, a proportional increase in the density of samples occurred from 0.75 at 0.5 wt.% to 0.93 at 5 wt.% of ZnAc (Figure 11c).



**Figure 11.** Relative density of ceramics vs. ZnAc concentration for different types of die sealing in CSP: single copper sealing, 1C (a); double copper sealing, 2C (b); double PTFE sealing, 2P (c).

Figures 12 and 13 showed the microstructures of ZnO ceramics prepared by CSP of ZnO@ZnAc and ZnO@ZnAcTVT powders, respectively, with double PTFE sealing. The fracture surfaces of the samples processed with the addition of 0.5 wt.% of ZnAc (Figures 12a and 13a) resembled the morphology of the corresponding powders (Figures 4a and 5a). With a higher content of ZnAc in the powders, coarse grain boundaries manifested, and a pronounced grain growth occurred (Figures 12b,c and 13b,c). However, fine grains corresponding to the fine component of powder size distribution are still noticed between the grown ones (Figure 13b,c). The dense sintered ceramics microstructure is observed in CSP samples, obtained from impregnated powder starting with a 2.5 wt.% ZnAc concentration (Figure 12b,c), for CSP TVT samples only for 5 wt.% ZnAc concentration (Figure 13c).



**Figure 12.** SEM images of ZnO ceramics prepared from powder impregnated by 0.5 wt.% ZnAc (a), 2.5 wt.% ZnAc (b), 5.0 wt.% ZnAc (c) (case of 2P sealing type during CSP).

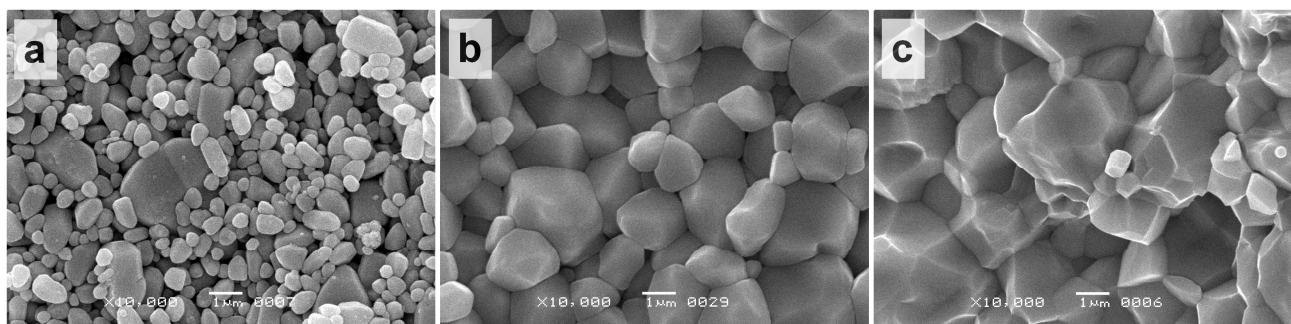


**Figure 13.** SEM images of ZnO ceramics prepared from powder impregnated by 0.5 wt.% ZnAc (a), 2.5 wt.% ZnAc (b), 5.0 wt.% ZnAc (c) and underwent TVT (case of 2P sealing type during CSP).

### 3. Discussion

Morphological and microstructural evolution of ZnO powder and ceramics in water medium observed in the current work was caused to a great extent by the presence of ZnAc. Early experiments performing CSP of ZnO in pure water demonstrated low effectiveness of this medium because of the low rate of interaction between ZnO and H<sub>2</sub>O [17].

In this study, the reaction medium contains an AcZn additive applied to a ZnO initial powder; when activated by CSP, this led to the formation of high-density ceramics. Two methods of activating by ZnO impregnation and TVT transferred the initial powder to a different state. When applying AcZn from an aqueous solution, an admixture of the LBZA phase appeared. The result of the TGA of the ZnO@AcZn sample with 5% additive (Figure 1a) showed a picture of thermal processes that was different from the TGA of AcZn [18] and close to the decomposition of LBZA [19,20]. It is known that the thermal decomposition of AcZn depends on the environment [21,22] and that TGA in an inert gas stream begins with dehydration at 76 °C. Then, melting takes place at about 245 °C, sublimation of anhydrous AcZn and its decomposition at 310 °C into acetone and carbon dioxide. However, when anhydrous AcZn was heated in a humid atmosphere ( $P_{\text{H}_2\text{O}} = 6 \text{ kPa}$ ), the formation of ZnO with the release of acetic acid was observed [22]. The thermal process started at 120 °C and ended at 220 °C.

Thermal analysis of the ZnO@AcZnTVT sample with 5% additive (Figure 2b) revealed that the formation of an associate of hydroxyl and acetate groups during TVT, which decomposes at about 200 °C. A small amount of the 2.34% associate makes it possible to associate it with the powders and ceramics observed on XRD patterns (Figures 2 and 7). Diffraction patterns show weak reflexes of an unidentified phase. This associate can be compared with hydroxyl associates involved in the exchange of water molecules between crystals and the aqueous medium [11]. This conclusion corresponds to the conclusion of [4] the appearance of ZnO acetate ions in the crystal structure during TVT and their participation together with hydroxyl groups in the exchange with the surrounding aqueous medium. The increased intensity of metabolic processes leads to an increase in structural mobility and mass transfer between crystals. The narrow endothermal effects at 117 °C and 151 °C (Figure 2b) of water release at TGA of the ZnO@AcZnTVT sample refer to the states of hydroxyl groups on the path of the transition of water molecules into the structure of ZnO crystals and back into the aqueous medium [11]. It should be noted that the width of the endothermal effects characterizes the uniformity of the decaying states. The narrow width of the endothermal effects noted above corresponds to the energy uniformity of hydroxyl groups. The narrow endoeffect in Figure 2a refers to the decomposition of the LBZA phase with atoms in certain crystallographic positions. The broader endothermal effect in Figure 2b characterizes the spread of the energy states of the hydroxyl–acetate associate. The narrowing of the endoeffect of the decomposition of the associate and the shift towards an increase in temperature by 60 °C is probably caused by a higher CSP temperature relative to the TVT activation temperature of ZnO—244 °C and 220 °C, respectively. An increase in the temperature of the interaction of crystals with the aqueous

medium leads to a decrease in the number of defects in their structure. The defects in this case are acetate groups.

The formation of the fine crystals during ZnO powder impregnation by AcZn (Figure 4) and the separation of the size ranges of small and large crystals with TVT (Figure 5) and during CSP of impregnated powder (Figure 8) is associated with surface processes [11,13]. In the case of impregnation and TVT, new fine crystals are formed, and in the case of CSP, the diffusion transfer of mass between the initial crystals leads to an increase in their size. The formation of crystals of a finely dispersed component was observed earlier, both during the activation of processes with the addition of AcZn or CH<sub>3</sub>COOH, and with the addition of NH<sub>4</sub>Cl [11,13]. In addition, the appearance of a finely dispersed component was detected during recrystallization of  $\alpha$ -Al<sub>2</sub>O<sub>3</sub> [23]. An increase in the size range of the fine component, noted in the commentary to Figure 9, was also observed in the study of ZnO recrystallization in the presence of NH<sub>4</sub>Cl [13] and in the study of the effect of mechanical pressure on ZnO recrystallization at CSP [11]. This effect can be associated with an increase in the thickness of the surface layer with increased solid-phase mobility.

The obtained results show the influence of two threshold concentrations of the activating additive. Exceeding the first threshold ensures the appearance of the crystal structure mobility, due to which the formation of a small component of the crystal size distribution and the growth of crystals of a large component occurs. When the second threshold is exceeded, crystal coalescence becomes possible during CSP [11]. Thus, when the content of the AcZn additive increases to 2.5% and 5% the CSP of the ZnO@AcZn and ZnO@AcZnTVT powders leads to the formation of dense ceramics (Figure 11) with large grains (Figures 12 and 13) due to coalescence. The existence of the second threshold of sintering activation is probably due to the condition of increasing the structural mobility to a level at which the preorientation of neighboring crystals becomes possible in order to achieve the crystallographic correspondence necessary for coalescence [24]. The reorientation of neighboring crystals can be explained by the diffusion mechanism of crystal rearrangement due to the solid-phase mobility of the structure. With crystallographic matching, the disappearance of the intergrain boundary becomes possible [25].

The effects of sealing materials on ceramics formation were caused by the difference of the state of water during the CSP. Double copper sealing (2C) provided maximum hermitization of the die but hampered sliding of the copper rings along the die wall. This resulted in the increase of the applied mechanical pressure. Removal of the excessive water at the final stage of sintering appeared difficult. Simultaneously, the mechanical pressure exceeded the autogenous pressure of vapor and caused its condensation.

When water filled the gaps between the crystals, its incompressibility ceased the shrinkage of the sample, and mechanical pressure lost its effectiveness. ZnO crystals appeared to be separated by incompressible water. This did not interfere with their growth due to mass transfer. Increased pressure of the aqueous medium led to intensified exchange of water molecules between it and the crystals and increased their structural mobility. This is favorable to crystal growth but obstructed coalescence, leading to low-density ceramics.

In a case of single copper sealing (1C), the powder was compressed but the pressure of the aqueous medium reduced because of water and steam escaping from the working volume through the gap between the punches and the die matrix. The permeability of this gap might be decreased when filled with powder, especially with fine crystals. For this reason, reproducibility of CSP conditions can lose its effectiveness. Besides, the reduced pressure of the aqueous medium inhibits mass transfer and crystal growth.

CSP conditions allowed by double PTFE sealing (2P) were determined by the softening of PTFE at a temperature of 244 °C. PTFE rings offered weak resistance to punch movement. Mechanical pressure affected the powder, while the pressure of the aqueous medium was determined by the elastic properties of the softened PTFE. Though water was partially bled off, the pressure of water vapor, which is in equilibrium with liquid water, was maintained in the working volume of the die. Mass transfer conditions were reproducible and close to TVT conditions. Features of sealing with PTFE rings determined the advantage of the

2P method such as the highest values of density with its clear proportionality to the ZnAc content as well as controllable grain size over a wide range.

#### 4. Materials and Methods

ZnO powder with the median particle size of 0.174  $\mu\text{m}$  and mean particle size of  $0.193 \pm 0.002 \mu\text{m}$  was used as a raw material for ceramics (>99% purity, JSC Krasnyi Khimik, Saint-Petersburgh, Russia). Zinc acetate dihydrate ( $\text{Zn}(\text{CH}_3\text{COO})_2 \cdot 2\text{H}_2\text{O}$ , ZnAc, >99% purity) was selected as an activating additive to ZnO powder.

Activation of the initial ZnO powder was carried out in two ways (Figure 14). The first way included ultrasonication of ZnO powder in ZnAc water solution followed by evaporation and drying in air at 70  $^\circ\text{C}$  for 12 h. The obtained ZnO impregnated by ZnAc (ZnO@ZnAc) was ground in an agate mortar with a pestle and sieved through a sieve with a cell of 300  $\mu\text{m}$ . ZnAc concentrations in the solutions supported zinc acetate contents in ZnO@ZnAc samples of 0.5; 2.5 and 5.0 wt.% (0.185; 0.927 and 1.853 mol.%, correspondingly). Another way of activation consisted of the impregnation procedure described above followed by a treatment of ZnO@ZnAc in water vapor (thermo-vaporous treatment, TVT). ZnO@ZnAc powder was placed into a PTFE container supported inside the stainless-steel autoclave. An amount of distilled water equal to 20% of the free volume of the autoclave was poured outside the PTFE container. The autoclave was sealed and heated up to 220  $^\circ\text{C}$ . ZnO@ZnAc powder was held in vapor state at 220  $^\circ\text{C}$  and 2.32 MPa for 20 h.

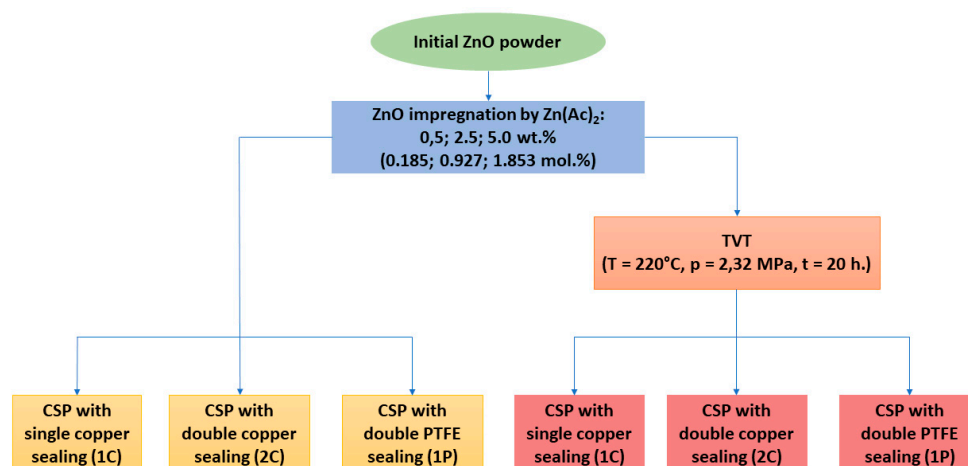


Figure 14. Scheme of ZnO powder preparation and cold sintering process conditions.

CPS was carried out in an induction heating stainless-steel die with four punches of 11 mm diameter. The powder was placed between a couple of inner punches which contacted with the outer ones either directly or through a sealing made of copper or PTFE. The role of the sealing was to prevent the extrusion or evaporation of water through the gaps in the die during pre-pressing and CPS.

Three types of the die hermitization were applied:

- (1) a copper ring between one couple of outer and inner punches and no sealing between another couple of outer and inner punches (1C);
- (2) copper rings between outer and inner punches (2C);
- (3) PTFE rings between outer and inner punches (2P).

The die was filled with 1 g of activated ZnO powder and 0.2 mL of distilled water (Figure 15). Then, another couple of punches were installed either with the sealing or without it (Figure 15b). A thermocouple was placed in a recess close to the powder. The die with the heater was installed along the axis of the laboratory hydraulic press (Figure 15a). To control the powder shrinkage, an axial displacement of the bottom platform of the press was measured by a dial indicator (value of division 10  $\mu\text{m}$ ). The regimen of CSP was chosen

based on previous results [14,26]: heating from the room temperature to 244 °C in 40 min., the dwell time of 60 min. at 244 °C. The heating started when a pressure of 395 MPa was reached. The permissible load on the equipment was selected in the preliminary tests.

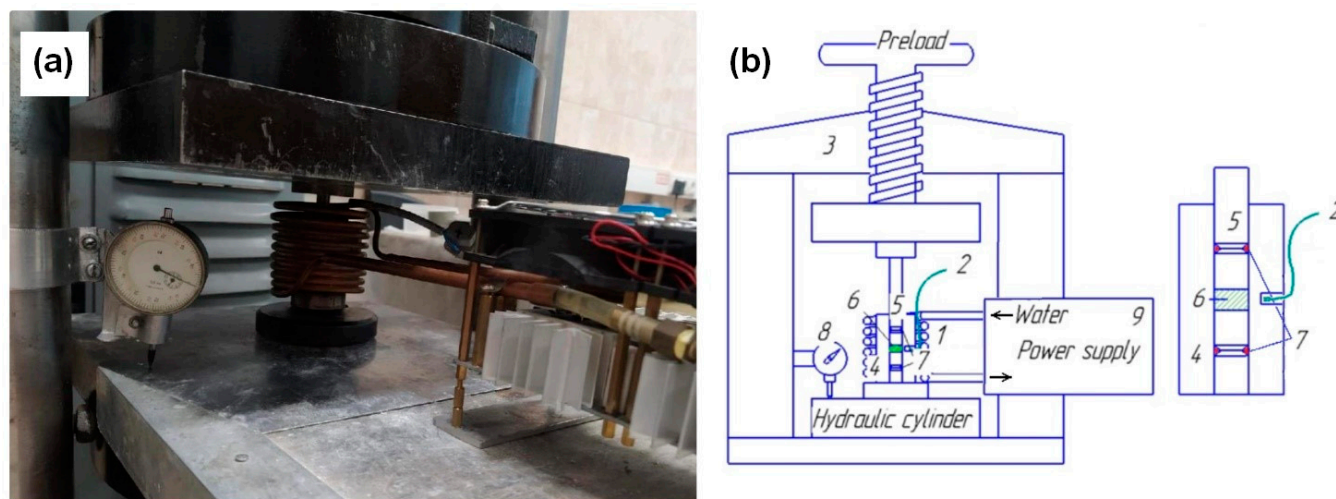


**Figure 15.** Equipment for cold sintering process (a) and its scheme (b): 1—induction heating; 2—thermocouple; 3—hydraulic press; 4—press form; 5—set of punches; 6—ZnO powder; 7—sealing; 8—sensor; 9—power supply.

Thermal analysis and mass-spectrometry of powder and ceramic samples was carried out in a Netzsch STA 449 C Jupiter thermal analyzer. The samples were heated in argon with the rate of 10°/min from 40 to 600 °C. X-ray diffraction analysis of the initial and activated powders as well as of ceramic samples was conducted by means of X-ray diffractometer XRD 6000 (Shimadzu Corp., Japan). Powder morphology and ceramics microstructure were investigated by a scanning electron microscope (SEM) JSM-6390 LA (JEOL Ltd., Japan). Size distributions of the powder particles and ceramic grains were constructed from the direct measurements of corresponding objects in the SEM images using Image-Pro Plus software (Media Cybernetics, Inc., USA). Size distributions were characterized by the mean value ( $d_{mn}$ ) as well as by the median ( $d_{md}$ ) which appears more adequate for an asymmetric distribution. Relative density of ceramics was determined at  $20 \pm 2$  °C and  $60 \pm 5\%$  relative humidity by Archimedes method using kerosene.

## 5. Conclusions

Two methods of zinc acetate introduction into ZnO powder by impregnation and TVT lead to various changes in its state and activity during cold sintering.

The powder activation by the impregnation method makes it possible to obtain cold sintered ceramics at 244 °C with a relative density of 0.98–0.99 and average grain sizes from 0.28 to 0.45 microns. When the powder is activated by TVT, the relative density of the ceramics increases from 0.75 to 0.93 with a change in the average grain size in the range of 0.46–1.71 microns with an increase in the content of zinc acetate additive from 0.5% to 5%. Of the three ways to seal the mold, the use of two Teflon sealing rings turned out to be optimal.

The explanation of the processes occurring in the TVT and CSP of ZnO powders is based on the idea of justifying the crystal's structure solid-phase mobility due to the interaction with an aqueous medium.

**Author Contributions:** Conceptualization, A.V.S. and Y.D.I.; methodology, A.A.K., E.V.F. and Y.D.I.; formal analysis, A.V.S., A.A.K., E.V.F. and Y.D.I.; investigation, M.V.K., S.A.M. and A.D.S.; resources, A.V.S.; data curation, M.V.K., S.A.M. and A.D.S.; writing—original draft preparation, A.V.S., M.V.K., A.A.K. and Y.D.I.; writing—review and editing, A.V.S., A.A.K. and Y.D.I. All authors have read and agreed to the published version of the manuscript.

**Funding:** This research was funded by RTU MIREA (initiative research “Ceramics Synthesis”).

**Data Availability Statement:** The data presented in this study are available on request from the corresponding author after obtaining the permission of an authorized person.

**Acknowledgments:** The work was carried out with the use of equipment of the Centre of Collective Usage «Joint Educational and Scientific Center for Collective Use» of MIREA—Russian Technological University (Agreement No. 075-15-2021-689). This work was supported in part by M.V. Lomonosov Moscow State University Program of Development. The authors are thankful to S.Yu. Kupreenko from Chemistry Department of Lomonosov MSU for his help in TG/DSC/MS analysis.

**Conflicts of Interest:** The authors declare no conflict of interest.

## References

1. Grasso, S.; Biesuz, M.; Zoli, L.; Taveri, G.; Duff, A.I.; Ke, D.; Jiang, A.; Reece, M.J. A Review of Cold Sintering Processes. *Adv. Appl. Ceram.* **2020**, *119*, 115–143. [[CrossRef](#)]
2. Guo, J.; Guo, H.; Baker, A.L.; Lanagan, M.T.; Kupp, E.R.; Messing, G.L.; Randall, C.A. Cold Sintering: A Paradigm Shift for Processing and Integration of Ceramics. *Angew. Chem. Int. Ed.* **2016**, *55*, 11457–11461. [[CrossRef](#)] [[PubMed](#)]
3. Maria, J.-P.; Kang, X.; Floyd, R.D.; Dickey, E.C.; Guo, H.; Guo, J.; Baker, A.; Funihashi, S.; Randall, C.A. Cold Sintering: Current Status and Prospects. *J. Mater. Res.* **2017**, *32*, 3205–3218. [[CrossRef](#)]
4. Ivakin, Y.D.; Smirnov, A.V.; Kurmysheva, A.Y.; Kharlanov, A.N.; Solís Pinargote, N.W.; Smirnov, A.; Grigoriev, S.N. The Role of the Activator Additives Introduction Method in the Cold Sintering Process of ZnO Ceramics: CSP/SPS Approach. *Materials* **2021**, *14*, 6680. [[CrossRef](#)] [[PubMed](#)]
5. Liang, J.; Zhao, X.; Kang, S.; Guo, J.; Chen, Z.; Long, Y.; Zeng, Q.; Sun, J.; Yang, L.; Liao, R.; et al. Microstructural Evolution of ZnO via Hybrid Cold Sintering/Spark Plasma Sintering. *J. Eur. Ceram. Soc.* **2022**, *42*, 5738–5746. [[CrossRef](#)]
6. Biesuz, M.; Grasso, S.; Sglavo, V.M. What’s New in Ceramics Sintering? A Short Report on the Latest Trends and Future Prospects. *Curr. Opin. Solid State Mater. Sci.* **2020**, *24*, 100868. [[CrossRef](#)]
7. Kang, X.; Floyd, R.; Lowum, S.; Cabral, M.; Dickey, E.; Maria, J. Mechanism Studies of Hydrothermal Cold Sintering of Zinc Oxide at near Room Temperature. *J. Am. Ceram. Soc.* **2019**, *102*, 4459–4469. [[CrossRef](#)]
8. Ndayishimiye, A.; Sengul, M.Y.; Bang, S.H.; Tsuji, K.; Takashima, K.; Hérisson de Beauvoir, T.; Denux, D.; Thibaud, J.-M.; van Duin, A.C.T.; Elissalde, C.; et al. Comparing Hydrothermal Sintering and Cold Sintering Process: Mechanisms, Microstructure, Kinetics and Chemistry. *J. Eur. Ceram. Soc.* **2020**, *40*, 1312–1324. [[CrossRef](#)]
9. Floyd, R.D.; Lowum, S.; Maria, J.-P. Cold Sintering Zinc Oxide with a Crystalline Zinc Acetate Dihydrate Mass Transport Phase. *J. Mater. Sci.* **2020**, *55*, 15117–15129. [[CrossRef](#)]
10. Chaim, R.; Levin, M.; Shlayer, A.; Estournes, C. Sintering and Densification of Nanocrystalline Ceramic Oxide Powders: A Review. *Adv. Appl. Ceram.* **2008**, *107*, 159–169. [[CrossRef](#)]
11. Ivakin, Y.D.; Smirnov, A.V.; Kormilitsin, M.N.; Kholodkova, A.A.; Vasin, A.A.; Korniyushin, M.V.; Tarasovskii, V.P.; Rybal’chenko, V.V. Effect of Mechanical Pressure on the Recrystallization of Zinc Oxide in a Water Fluid Medium under Cold Sintering. *Russ. J. Phys. Chem. B* **2021**, *15*, 1228–1250. [[CrossRef](#)]
12. Ivakin, Y.; Smirnov, A.; Kholodkova, A.; Vasin, A.; Kormilitsin, M.; Korniyushin, M.; Stolyarov, V. Comparative Study of Cold Sintering Process and Autoclave Thermo-Vapor Treatment on a ZnO Sample. *Crystals* **2021**, *11*, 71. [[CrossRef](#)]
13. Ivakin, Y.D.; Danchevskaya, M.N.; Muravieva, G.P. Recrystallization of Zinc Oxide in a Sub- and Supercritical Water Medium. *Russ. J. Phys. Chem. B* **2019**, *13*, 1189–1200. [[CrossRef](#)]
14. Ivakin, Y.D.; Smirnov, A.V.; Tarasovskii, V.P.; Rybal’chenko, V.V.; Vasin, A.A.; Kholodkova, A.A.; Kormilitsin, M.N. Cold Sintering of ZnO Ceramic in Water Medium: Test Demonstration. *Glass Ceram.* **2019**, *76*, 210–215. [[CrossRef](#)]
15. Tarat, A.; Nettle, C.J.; Bryant, D.T.; Jones, D.R.; Penny, M.W.; Brown, R.A.; Majitha, R.; Meissner, K.E.; Maffei, T.G. Microwave-Assisted Synthesis of Layered Basic Zinc Acetate Nanosheets and Their Thermal Decomposition into Nanocrystalline ZnO. *Nanoscale Res. Lett.* **2014**, *9*, 11. [[CrossRef](#)]
16. Vaitkus, A.; Merkys, A.; Gražulis, S. Validation of the Crystallography Open Database Using the Crystallographic Information Framework. *J. Appl. Crystallogr.* **2021**, *54*, 661–672. [[CrossRef](#)]
17. Ndayishimiye, A.; Fan, Z.; Funahashi, S.; Randall, C.A. Assessment of the Role of Speciation during Cold Sintering of ZnO Using Chelates. *Inorg. Chem.* **2021**, *60*, 13453–13460. [[CrossRef](#)] [[PubMed](#)]
18. Duan, Y.; Li, J.; Yang, X.; Hu, L.; Wang, Z.; Liu, Y.; Wang, C. Kinetic Analysis on the Non-Isothermal Dehydration by Integral Master-Plots Method and TG–FTIR Study of Zinc Acetate Dihydrate. *J. Anal. Appl. Pyrolysis* **2008**, *83*, 1–6. [[CrossRef](#)]

19. Moezzi, A.; McDonagh, A.; Dowd, A.; Cortie, M. Zinc Hydroxyacetate and Its Transformation to Nanocrystalline Zinc Oxide. *Inorg. Chem.* **2013**, *52*, 95–102. [[CrossRef](#)]
20. Poul, L.; Jouini, N.; Fiévet, F. Layered Hydroxide Metal Acetates (Metal = Zinc, Cobalt, and Nickel): Elaboration via Hydrolysis in Polyol Medium and Comparative Study. *Chem. Mater.* **2000**, *12*, 3123–3132. [[CrossRef](#)]
21. Ghule, A.V.; Ghule, K.; Chen, C.-Y.; Chen, W.-Y.; Tzing, S.-H.; Chang, H.; Ling, Y.-C. In Situ Thermo-TOF-SIMS Study of Thermal Decomposition of Zinc Acetate Dihydrate. *J. Mass Spectrom.* **2004**, *39*, 1202–1208. [[CrossRef](#)]
22. Aii, T.; Kishi, A. The Effect of Humidity on Thermal Process of Zinc Acetate. *Thermochim. Acta* **2003**, *400*, 175–185. [[CrossRef](#)]
23. Ivakin, Y.D.; Danchevskaya, M.N. Analysis of Recrystallization of Fine-Crystalline Corundum in a Supercritical Water Medium Using the Lognormal Particle Size Distribution Function. *Russ. J. Phys. Chem. B* **2018**, *12*, 1205–1211. [[CrossRef](#)]
24. Leite, E.R.; Giraldo, T.R.; Pontes, F.M.; Longo, E.; Beltrán, A.; Andrés, J. Crystal Growth in Colloidal Tin Oxide Nanocrystals Induced by Coalescence at Room Temperature. *Appl. Phys. Lett.* **2003**, *83*, 1566–1568. [[CrossRef](#)]
25. Theissmann, R.; Fendrich, M.; Zinetullin, R.; Guenther, G.; Schierning, G.; Wolf, D.E. Crystallographic Reorientation and Nanoparticle Coalescence. *Phys. Rev. B* **2008**, *78*, 205413. [[CrossRef](#)]
26. Funahashi, S.; Guo, J.; Guo, H.; Wang, K.; Baker, A.L.; Shiratsuyu, K.; Randall, C.A. Demonstration of the Cold Sintering Process Study for the Densification and Grain Growth of ZnO Ceramics. *J. Am. Ceram. Soc.* **2017**, *100*, 546–553. [[CrossRef](#)]